Research paper

Effects of the cation ordering in Mg:Al and Zn:Al layered double hydroxides on crystallographic and spectroscopical properties by means of first principles calculations

Carlos Pimentel [a,1], Alexander Pérez de la Luz [a,b], Alfonso Hernández-Laguna [a], C. Ignacio Sainz-Díaz [a,*]

[a] *Instituto Andaluz de Ciencias de la Tierra, Consejo Superior de Investigaciones Científicas-Universidad de Granada, Av. de las Palmeras, 4, 18100 Armilla, Granada, Spain*
[b] *Departamento de química, Universidad Autónoma Metropolitana-Iztapalapa, Av. San Rafael Atlixco, 186, col. Vicentina, 09340 Ciudad de México, Mexico*

ARTICLE INFO

ABSTRACT

Layered double hydroxides (LDH) are interesting materials due to their high absorption and catalytic properties. Their applications in environment, agriculture and pharmaceutical fields are becoming widely important. The interlayer and intralayer cation ordering on layered double hydroxides of Mg:Al 2:1 and Zn:Al 2:1 are studied by means of different ordering models at Density Functional Theory level. The cation ordering in LDH is interesting for monitoring the synthesis of these solids and for the applications of LDH, however it is difficult to determine experimentally. We have explored several ordering arrangements of the cation distribution in Mg:Al 2:1 and Zn: Al 2:1 LDH and the effect of these cation arrangements on some crystallographic and spectroscopic properties.

1. Introduction

The layered double hydroxides (LDH) are metal hydroxides forming lamelar structures. LDH are structurally related with brucite, $Mg(OH)_2$, where Mg cations are substituted by different relative proportions of other cations and vacancies. LDHs can be generally described using the following chemistry formula (Krivovichev et al., 2010; Andre et al., 2015):

$$\left[M^{2+}_{(1-x)} M^{3+}_x (OH)_2 \right]^{x+} \left[A^{n-}_{x/n} \cdot z\, H_2O \right]^{x-}$$
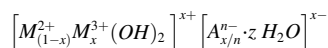
where $M^{2+} = Mg^{2+}$, Zn^{2+}, Fe^{2+}...; $M^{3+} = Al^{3+}$, Fe^{3+}, Cr^{3+}...; A^{n-} is a charge balance anion (e.g., Cl^-, CO_3^{2-}, SO^{2-}), x is the cationic layer charge and z is the amount of water molecules in the interlayer.

The layers are positively charged and anions are intercalated in the interlayer space for neutralizing the layered charge excess. These anions can be exchanged by other inorganic and organic anions (Miyata, 1983; Cavani et al., 1991). This property provides important adsorption capacity to these minerals, acting as an inorganic membrane. This behaviour and the small particle size are some characteristics because of

they are considered within the clay minerals group (Forano et al., 2006), although LDH are not silicate compounds. These minerals provide confined spaces in the interlayer zones, which along with the selective membrane behaviour and the energy provided by the electrostatic interactions from the charge gradient offer a scenario for the first prebiotic reactions, which could be critical for the origin of life (Greenwell and Coveney, 2006; Duval et al., 2019).

LDHs are easily synthesized in the laboratory and their description can be found in numerous papers (Forano et al., 2006; Figueiredo et al., 2018). However, it is difficult to determine experimentally how the cations are distributed in the crystal structure due to their small crystal domains and stacking disorder (Krivovichev et al., 2010; Zhitova et al., 2010). The knowledge of the cation ordering can be useful for monitoring the synthesis process of these solids, and also for evaluating their catalytic activity regarding to the distribution and segregation of the active sites.

Cation ordering in minerals is interesting for crystallographic analysis, for crystal growth, crystal stability and for industrial applications. The formation of synthetic minerals is produced in reaction rates much faster than the formation of natural minerals. Some synthetic minerals

---

* Corresponding author.
E-mail address: ci.sainz@csic.es (C.I. Sainz-Díaz).
[1] Current address: Université Grenoble Alpes, CNRS, ISTerre, 38000 Grenoble, France.

had not enough time for equilibrating into a minimal energy state. This fact affects some properties of the minerals especially the cation ordering, and their properties derived. Then, the cation ordering has great interest for thermodynamic models of mineral formation and as petrogenetic indicators. In last decades, many efforts have been made in cation ordering of clay minerals (Cuadros et al., 1999; Sainz-Díaz et al., 2000; Plançon, 2001; Botella et al., 2004; Palin et al., 2004; Mercier et al., 2005; Ortega-Castro et al., 2009), other silicates (Warren et al., 2001) and other minerals, such as carbonates (Hammouda et al., 2011; Pimentel et al., 2021) and also LDHs (Braterman and Cygan, 2006; Costa et al., 2010, 2011; Zhitova et al., 2010; Cadars et al., 2011; Liu et al., 2020).

Cation and anion ordering on LDH structures has been previously experimentally studied finding discrepancies between different studies (Hofmeister and Platen, 1992; Evans and Slade, 2006; Krivovichev et al., 2010). Krivovichev et al. (2010) found ordered cation structure in natural $Mg_2Al(CO_3)$ LDH samples, whereas Zhitova et al. (2010) found similar natural LDH with disordered cation distribution probably by a higher temperature formation. For instance, Kruissink et al. (1981) and Vucelic et al. (1997) reported a random cation distribution in LDH structures, whereas Sideris et al. (2008) found by Nuclear Magnetic Resonance (NMR) studies that in LDH cations are not randomly distributed. However, Vucelic et al. (1997) and Sideris et al. (2008) reported experimentally a common result, M^{3+} cations avoid close contacts, indicating that LDH could have local order, even if no long-range cation order is identified as other authors (Cadars et al., 2011; Figueiredo et al., 2021). In addition, Richardson and Braterman (2007) reported that LDH can be synthesized without cation ordering, although, due to an aging process, these structures can end up having cation ordering.

In order to try to shed light on this problem, some theoretical studies have been carried out on the LDH structures. However, in some of these works, the effect of the different cation arrangements, i.e. order-disorder, was not studied and the structures were considered to have the cations arranged only following the avoiding close contact principle (Wang et al., 2001, 2003; Lombardo et al., 2005, 2008; Costa et al., 2010, 2011; Jayanthi et al., 2017). Costa et al. (2010) calculated at DFT level the formation energy of carbonate-LDH from the pristine oxides, hydroxides and metal salts and water considering only the ordered cation distribution. On the other hand, Costa et al. (2011) studied by DFT calculations the hydration and dehydration process in Zn_2AlCl LDH with an ordered cation configuration. Molecular dynamics simulations based on empirical force fields of Zn_2AlCl LDH were used for determining the $d(003)$ and $d(006)$ spacings in X-Ray diffraction (XRD) patterns (Pisson et al., 2008). These authors compared two cation distributions, one 2D ordered and one disordered, finding that the cation ordering affects the structural and dynamical properties of the intercalated anions and water species. DFT calculations have been applied for studying the polytypism of LDH (Moraes et al., 2019). However, to the best of our knowledge, a theoretical study considering both 2-D and 3-D cation arrangements between the intralayer and interlayer cation ordering would be interesting.

Taking into account the discrepancies on cation order in the literature and the importance of cation order for the industrial applications of LDHs, this work aims to shed light on the cationic ordering by means of modelling at first principles level. Therefore, it has been determined which orderings are energetically more favourable. In addition, new methods are provided for helping the experimental identification of the ordering degree of cations by obtaining theoretical diffractograms and vibrational-spectra.

2. Models

The LDH models were taken from previous experimental crystallographic data of hydrotalcite, $Mg_6Al_2(CO_3)(OH)_{16} \cdot 4H_2O$ (Allmann and Jepsen, 1969). This experimental formula has been changed according to the following features: i) the $Mg^{2+}:Al^{3+}$ ratio was changed from 3:1 to 2:1; ii) carbonate groups were removed and substituted by Cl anions, one anion per aluminium cation in the structure, in order to maintain the electroneutrality of the structure in the interlayer space of the three layers; iii) some models were considered anhydrous, i.e., where water molecules were also removed from the structure; and iv) in order to study the Zn-LDH, Mg^{2+} cations were substituted by Zn^{2+} cations. So, the model formula is either $Mg_4Al_2(Cl_2)(OH)_{12}$ or $Zn_4Al_2(Cl_2)(OH)_{12}$.

A LDH 2x3x1 supercell was constructed for both Mg-LDH and Zn-LDH. The Al^{3+} cations substitutions were firstly placed tending a maximal dispersion along each octahedral sheet. Taking into account that the unit cell comprises 3 layers, different ordering of Al^{3+} cations models were considered (Fig. 1). The substitution of Al^{3+} cations in the LDH layers were followed by the introduction of Cl^- anions between the interlayers. The minimum and maximum number of Cl^- anions considered in the interlayers was 0 and 4 per interlayer, respectively. The hydrated models were generated placing a minimal water content in the interlayer space, such as, three molecules in each interlayer space per supercell. Initially, each water molecule was placed in the centre of the interlayer space, in a parallel orientation with respect to the *ab* plane, i.e. (001), and maximally dispersed along the supercell with the H atoms oriented towards the chloride anions and the O atoms close to the H atoms of the hydroxyl groups of the mineral surface.

A Mg-LDH 4x6x1 supercell was also constructed to study the effect of

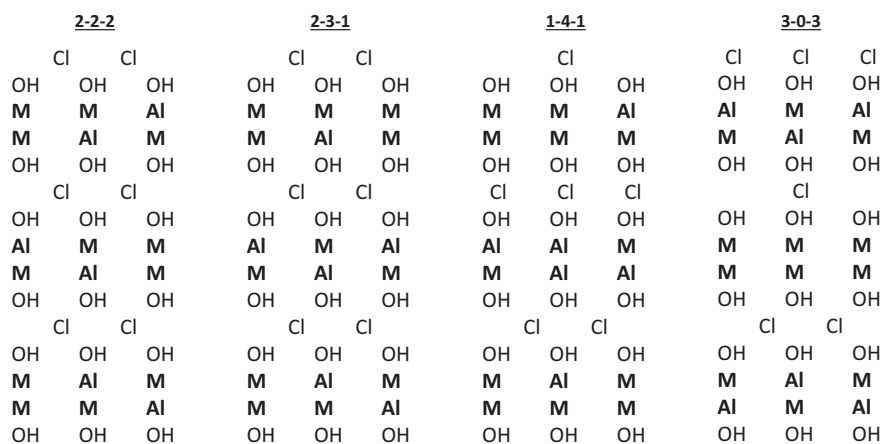**Fig. 1.** Scheme of several cation distributions of 2x3x1 LDH structure considered in this study: 2-2-2 (homogeneous distribution of Al cations), 2-3-1, 1-4-1 and 3-0-3, being each digit the number of Al^{3+} in each layer. M denotes both Magnesium and Zinc atoms for Mg-LDH and Zn-LDH, respectively. Al denotes aluminium atoms, Cl denotes chlorine atoms and OH denotes the OH layers both above and below the cationic layers.
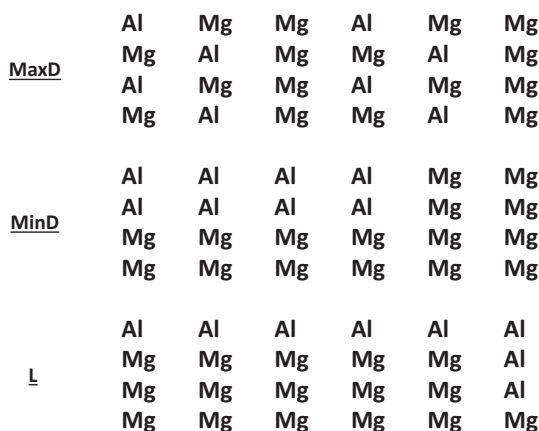
MaxD	Al	Mg	Mg	Al	Mg	Mg
	Mg	Al	Mg	Mg	Al	Mg
	Al	Mg	Mg	Al	Mg	Mg
	Mg	Al	Mg	Mg	Al	Mg
MinD	Al	Al	Al	Al	Mg	Mg
	Al	Al	Al	Al	Mg	Mg
	Mg	Mg	Mg	Mg	Mg	Mg
	Mg	Mg	Mg	Mg	Mg	Mg
L	Al	Al	Al	Al	Al	Al
	Mg	Mg	Mg	Mg	Mg	Al
	Mg	Mg	Mg	Mg	Mg	Al
	Mg	Mg	Mg	Mg	Mg	Mg

Fig. 2. Scheme of the distributions of Mg and Al in the second cationic layer of the Mg-LDH: maximum dispersion (MaxD), minimum dispersion (MinD) and all cations in line (L).

the intralayer cationic order. In this case, three different arrangement of Al^{3+} cations were considered in the second cationic layer (Fig. 2): i) maximum dispersion (MaxD); ii) all cations segregated (minimum dispersion) (MinD); and iii) all cations in line (L).

3. Methodology

Preliminary calculations were performed exploring different force fields (FF). However, in the optimization at variable cell the cations lose the coplanarity that could alter our studies of cation ordering (see Fig. S1 in Supplementary Support). Such alterations of the octahedral sheets had been also observed in previous theoretical studies conducted using molecular dynamics with FF (Wang et al., 2001; Lombardo et al., 2008; Pérez-Sánchez et al., 2018). In these cases, however, the deformations can even lead to bending the octahedral layers, due to the rearrangement of chlorine ions and water molecules in the interlayer (Lombardo et al., 2008; Pérez-Sánchez et al., 2018).

To overcome this alteration, quantum mechanical calculations based on Density Functional Theory (DFT) were used, applying 3-D periodical boundary conditions based on plane wave conditions, by using CASTEP (Clark et al., 2005), included in Materials Studio package (Biovia, 2018), and Quantum-Espresso (Giannozzi et al., 2009, 2017) codes with the generalized gradient approximation (GGA), and the Perdew-Burke-Ernzerhof functional (PBE) for the exchange-correlation potential (Perdew et al., 1996). The graphical analysis of crystal systems have been performed by using the VESTA (Momma and Izumi, 2011) and XCRYSDEN (Kokalj, 1999) software.

In the CASTEP calculations, on-the-fly generated (OTFG) ultrasoft pseudopotentials were used including Koelling-Harmon relativistic treatment (Vanderbilt, 1990). This computational approach was previously useful for study LDH (Liu et al., 2020; Li et al., 2021), and other minerals (Sainz-Díaz et al., 2004a, 2004b). Preliminary total energy calculations were performed at different values of energy cut-off in order to optimize the calculation parameters and to find the optimal value of energy cut-off for our mineral. We observed that the total energy decreases with the increase of energy cut-off until reaching a planar profile where the variation of total energy with respect to the energy cut-off is not significant (see Fig. S2a in Supplementary Support). This preliminary study allowed optimization of the calculation parameters in order to obtain the maximum precision and reliability of the simulation with the minimum computational cost. This cut-off was 571.4 eV and we considered this value for the rest of calculations in this work, although some further calculations were also carried out at a cut-off of 630 eV. All calculations were performed in the Γ point of the irreducible Brillouin zone of the crystal lattice. Besides, the effect of dispersion corrections from Grimme (2006) and Tkatchenko (Tkatchenko and Scheffler, 2009)

methods were compared fully optimizing the crystal structure including the atomic positions and the cell parameters. All structures of LDH with different cation ordering were optimized using the same calculation conditions and 2x3x1 supercell, except for the intralayer order simulations, which were performed using a 4x6x1 supercell with a cut-off of 489.8 eV. The powder X-ray diffraction patterns were simulated from the crystal structures using the REFLEX code (Biovia, 2018). Infrared and Raman vibration modes frequencies were calculated using CASTEP code (Clark et al., 2005). Prior to infrared and Raman calculations, the optimized structures were re-optimized with an energy cut-off of 630 eV, in order to avoid the presence of negative frequencies in the spectra. Subsequently, OTFG norm conserving pseudopotentials and an energy cut-off of 925.2 eV were used.

In the Quantum Espresso calculations, PAW (Projector Augmented Wave) pseudopotentials (Blöchl, 1994) and USPP (ultrasoft pseudopotentials) (Vanderbilt, 1990) were tested and we chose the PAW pseudopotentials because they allowed a better description of the experimental values of the cell parameters of these systems than with the USPP pseudopotentials. A preliminary study was also performed to find the optimal parameters and obtain the best precision at minimum computational cost. Different energy cut-off values were tested for finding the optimal calculation conditions. So, preliminary total energy calculations were performed with different values of energy cut-off E_{cut}(wfc) (40–140 Ry) (see Fig. S2b in Supplementary Support) and cut-off for the rho charge density (160–840 Ry) with different ratios of rho-cut-off/energy-cut-off (4–7) (Fig. S3). Initially the energy decreased drastically with the increase of energy cut-off, decreasing the slope of the profile until reaching a planar zone where the total energy becomes practically constant with the increase of energy cut-off. Then, the energy cut-off E_{cut}(wfc) used for crystal structures calculations was 100 Ry and with a charge density cut-off of 400 Ry in this work. This level is a good compromise between calculation level and computational effort. In addition, several k point grid samplings for the optimization of the Brillouin zone (Monkhorst and Pack, 1976) were explored, finding the optimal calculations conditions (see Table S1 in Supplementary Support) with 3x2x1 *k*-points grid. In all calculations dispersion corrections were included according to the DFT-D3 scheme (Grimme et al., 2010). Finally, the frequencies of the vibration normal modes of the optimized crystals were obtained from calculations based on the Density Functional Perturbation Theory (DFPT) (Baroni et al., 1987, 2001). The spectroscopical vibration modes were analysed by using the Molden code (Schaftenaar and Noordik, 2000).

4. Results and discussion

4.1. Optimization of LDH structures

The full optimization, atomic positions and lattice cell parameters, calculated with dispersion corrections yielded a crystal structure with closer cell parameter values to experimental data than without considering these corrections (Table 1). Therefore, the dispersion correction of

Table 1
Crystal structures of the 2x3x1 supercell of Mg-LDH (Mg:Al = 2:1) calculated without and with dispersion correction with CASTEP, comparing with experimental values (distances in Å and angles in °).

Parameters	Without correction	TS[a]	Grimme[b]	Exp[c]
a	3.090	3.064	3.060	3.04
b	3.083	3.056	3.054	3.04
c	22.48	22.154	22.259	23.0
α	89.8	89.7	89.6	90
β	90.0	90.1	90.1	90
γ	120.4	120.4	120.4	120

[a] Tkatchenko dispersion correction.
[b] Grimme dispersion correction.
[c] Experimental values from Figueiredo et al. (2021).
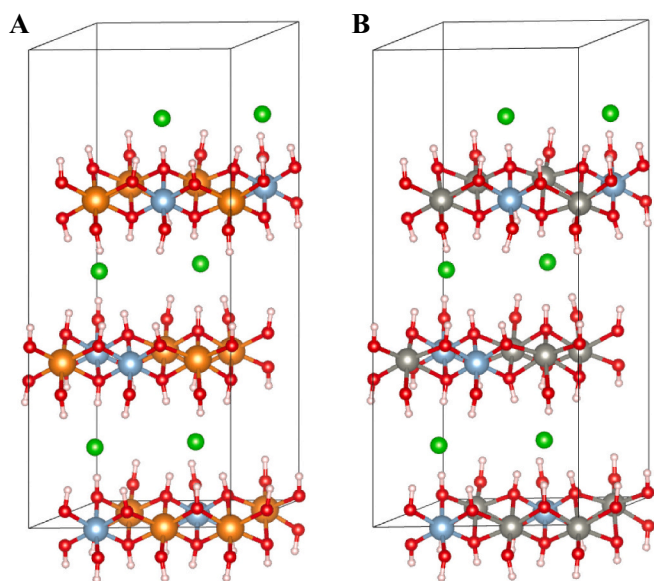
Fig. 3. Crystal structure of a 2x3x1 supercell of Mg-LDH (A) and Zn-LDH (B) optimized using CASTEP code. Two Al^{3+} cations can be found in each layer with a maximum dispersion. All the figures of structural models have been constructed using VESTA software (Momma and Izumi, 2011).

Table 2
Unit cell parameters of anhydrous Mg-LDH and Zn-LDH, with 2 Al^{3+} cations per layer, calculated using CASTEP and Quantum Espresso and compared with experimental data.

Parameters	Mg-LDH			Zn-LDH		
	CASTEP	QE	Exp[a]	CASTEP	QE	Exp[a]
a	3.060 (3.061)	3.075	3.04	3.131 (3.125)	3.123	3.08
b	3.054 (3.054)	3.066	3.04	3.114 (3.107)	3.100	3.08
c	22.259 (22.117)	22.020	23.0	22.287 (22.000)	21.950	23.22
α	89.6 (89.3)	89.6	90	89.3 (89.4)	89.8	90
β	90.1 (90.1)	90.0	90	90.0 (90.0)	89.9	90
γ	120.4 (120.4)	120.4	120	120.8 (120.7)	120.7	120
$d(003)$	7.42 (7.35)	7.33	7.67	7.43 (7.33)	7.32	7.73

In CASTEP parameters at two different cut-off are given: 571.4 eV and 630 eV (in brackets). All the distances are in Å and angles in °.
[a] Experimental values from Figueiredo et al. (2021).

Grimme was included in all calculations of this work.

Once determined the best theoretical approach to study the LDH structures, both Mg-LDH and Zn-LDH structures with an equal distribution and maximum dispersion of Al^{3+} cations on the 3 hydroxide layers, i.e. 2 Al^{3+} per layer, were optimized by relaxing atomic positions and crystal lattice (Fig. 3, Table 2). In both optimized LDH structures, i. e. Mg and Zn, the cell parameters agree with those reported for experimental LDH with the same $M^{2+}:Al^{3+}$ ratio (Ennadi et al., 2000; Lombardo et al., 2008; Mahjoubi et al., 2017; Figueiredo et al., 2021), with previous theoretical calculations of LDH (Andre et al., 2015), and with previous calculations using CASTEP on a monolayer brucite model (Liu et al., 2020). Comparing the results using both theoretical approximations, CASTEP and QE, both can be considered similar. No improvement was observed increasing the cut-off energy from 571.4 eV to 630 eV in the CASTEP calculations. As in the case of the experimental LDH, theoretical a and b parameters are slightly higher for Zn-LDH than for Mg-LDH, due to the higher ionic radii of Zn^{2+} compared to Mg^{2+} (Shannon, 1976). Moreover, almost all the cell angles can be considered

similar to the experimental ones. In both LDH structures, Mg-LDH and Zn-LDH, the H – O bonds have an average length of 0.981 and 0.982 Å for the 2-2-2 cation arrangement, respectively (see radial distribution function in Fig. S5). In general, the chloride anions are in the centre of the interlayer with an average d(Cl…HO) distances of 2.32 Å and 2.35 Å for Mg-LDH and Zn-LDH, respectively.

Nevertheless, the main differences between the theoretical and experimental results are in the c parameter, which are higher in the experimental LDH (Table 2). This difference is due to the different hydration state of the LDH, which are anhydrous in our calculations and hydrated in the experimental results. Therefore, 9 water molecules (3 per interlayer) were added to the 3x2x1 supercell of Mg-LDH and Zn-LDH, i.e. 1.5 water molecules per unit cell. After the optimization using both CASTEP and Quantum Espresso calculations (Fig. 4), c is higher in the hydrated phases (Table 3), while all other parameters remain close to the values of the anhydrous structure. These results are in good agreement with the experimental results previously reported (Miyata, 1983; Boclair et al., 1999; Ennadi et al., 2000; Lombardo et al., 2008; Mahjoubi et al., 2017; Figueiredo et al., 2021). However, there are still some differences in the c parameters between the theoretical and experimental structures, which are influenced by the total number of water molecules in the interlayers (Wang et al., 2001; Pisson et al., 2008). Moreover, as stated by Figueiredo et al., 2021, depending on the method used to calculate the hydrated structure, different amounts of water molecules will be needed to reach the c parameter measured on
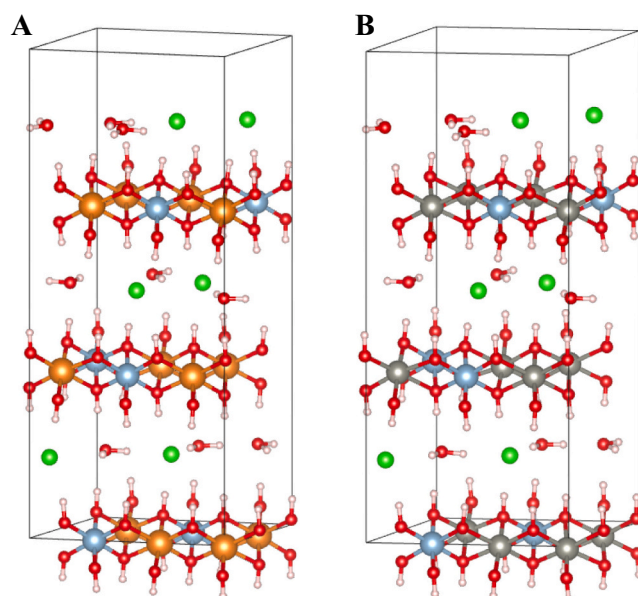
Fig. 4. Hydrated crystal structure of a 2x3x1 supercell of Mg-LDH (A) and Zn-LDH (B) optimized using CASTEP code. Two Al^{3+} cations and 3 water molecules can be found in each layer and interlayer, respectively.

Table 3
Hydrated LDH structures calculated using CASTEP and QE with 1.5 water molecules per unit cell.

Parameters	Mg-LDH hyd	Mg-LDH hyd	Zn-LDH hyd	Zn-LDH hyd
	CASTEP	QE	CASTEP	QE
a	3.081 (3.081)	3.086	3.140 (3.138)	3.120
b	3.070 (3.070)	3.079	3.121 (3.119)	3.103
c	23.630 (23.630)	23.241	23.267 (23.122)	23.110
α	92.2 (92.2)	90.3	91.0 (90.6)	90.8
β	88.4 (88.4)	90.0	89.3 (89.7)	89.8
γ	120.3 (120.7)	120.6	121.0 (120.9)	120.7
$d(003)$	7.87 (7.87)	7.75	7.75 (7.71)	7.70

In CASTEP two different cut-off were used: 571.4 eV and 630 eV (in brackets). All distances are in Å and angles in °.

the experimental LDH. In general, the water molecules remain close to the centre of the interlayer changing their positions from the initial one, being the distances between atoms in the interlayer of Mg-LDH and Zn-LDH structures the followings: d(Cl…OH) distance of 3.06 Å and 3.03 Å; d(H_2O…HOM) of 2.06 and 1.95 Å, and d(H_2O…Cl) of 2.89 Å and 2.65 Å.

Both anhydrous and hydrated LDH structures optimized using CASTEP and QE keep the coplanarity of the octahedral layers (Figs. 3 and 4), in contrast with the preliminary results obtained using FF of anhydrous LDH (Fig. S1). The aim of this work is to study the effect of the cation order in the LDH structures. It is therefore necessary that the layers and interlayers of the structures used are as unaltered as possible in order to be able to determine the real effect of the different cation arrangements, which, due to the lack of suitability of the FF methods, has led to the study of these phases using quantum mechanics calculations. Moreover, the obtained parameters and angles are close to those reported in the literature (for both theoretical and experimental LDH) and close to the hexagonal crystal system (i.e. $\alpha = \beta = 90°$ and $\gamma = 120°$), so, both calculation methods are validated to be used, since no symmetry constraints were imposed on these structures in both CASTEP and QE calculations. Then, the calculations of the different ordering of Al^{3+} cations were carried out by using only CASTEP with a cut-off of 571.4 eV.

4.2. Cation ordering on LDH structures

Once optimized the Mg-LDH and Zn-LDH structures with 2 Al^{3+} cations per octahedral layer (i.e. 2-2-2), three new structures with different Al^{3+} cation arrangements were created to study the effect of the cation order on LDH structures. Such structures were designed by moving the aluminium cations between the different layers, being as follows: 2-3-1, 1-4-1 and 3-0-3 (Fig. 1), each number indicates the number of Al^{3+} cations in each octahedral layer.

In all these structures with different Al^{3+} cation arrangements were also optimized at variable volume, and the *a* and *b* parameters remain quite close to the values of the initial structure, while *c* parameter was increased in the disordered structures compared to the initial structures (Tables 4 and 5). The highest *c* values in disordered LDH structures were

in the 1-4-1 one for both Mg-LDH (22.899 Å) and Zn-LDH (22.492 Å). However, these values cannot be compared to those obtained experimentally due to the different hydration states. Therefore, these values are a sign of the stresses to which the lattice is subjected with the various cation arrangements. Moreover, comparing the energies of the different structures, the initial ordered structure (i.e. 2-2-2) has the lowest energy and can be assumed to be the most probable cation arrangement to be found in LDH structures. On the contrary, 1-4-1 and 3-0-3 seems to be the less probable configurations to be found in LDH structures due to their highest energies because of the distortions produced on the octahedral layers (Fig. 5 and Fig. S4). The same phenomenon is found in both
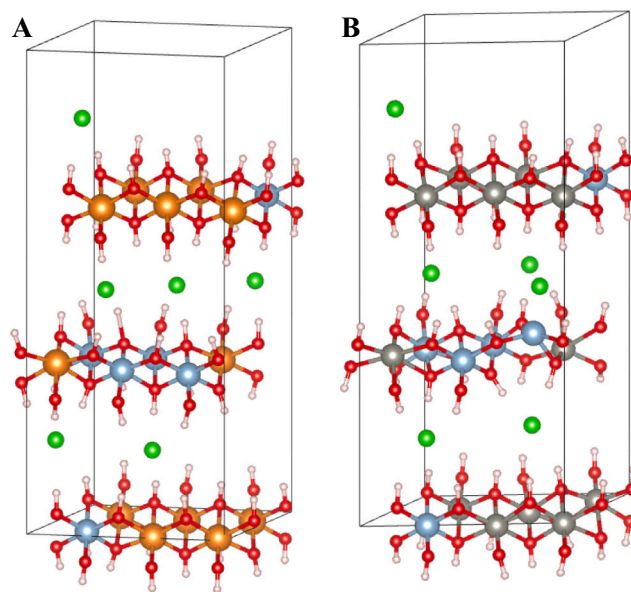

Fig. 5. Crystal structure of a 2x3x1 supercell of 1-4-1 of Mg-LDH (A) and Zn-LDH (B) optimized using CASTEP code. As can be seen in B, Zn-LDH shows a distorted octahedral layer in the sheet with 4 Al^{3+} cations.

Table 4
Interlayer Al^{3+} cation ordering in Mg-LDH.

Cation pattern	2-2-2	2-3-1		1-4-1			3-0-3	
Anion pattern	A222	A222	A231	A231	A141	A222	A312	A303
a	3.060	3.064	3.070	3.055	3.058	3.057	3.075	3.080
b	3.054	3.050	3.051	3.046	3.050	3.052	3.049	3.029
c	22.259	22.642	22.542	22.899	23.175	23.039	22.613	19.298
α	89.6	90.0	88.6	91.9	90.6	88.5	89.5	89.6
β	90.1	90.0	90.4	91.8	91.4	90.5	90.0	92.6
γ	120.4	120.4	120.3	120.2	119.3	120.2	120.5	120.1
energy	0	0.317	0.513	0.727	1.034	1.059	0.937	0.641
d(003)	7.42	7.55	7.51	7.62	7.72	7.68	7.54	6.42

Numbers indicate the number of Al cations in each LDH layer. The 2-2-2 one is the original structure optimized. Energy is the energy difference (in eV) per unit cell with respect to the lowest energy configuration. Distances are in Å, and angles in °.

Table 5
Interlayer Al^{3+} cation order in the Zn-LDH structure.

Cation pattern	2-2-2	2-3-1		1-4-1		3-0-3		
Anion pattern	A222	A222	A231	A231	A141	A312	A303	A222
a	3.131	3.130	3.139	3.095	3.107	3.147	3.147	3.106
b	3.114	3.098	3.100	3.106	3.131	3.101	3.093	3.113
c	22.287	22.472	22.620	22.492	22.970	22.402	21.576	22.554
α	89.3	90.0	88.0	89.1	85.8	92.1	88.3	90.2
β	90.0	90.1	91.0	90.9	90.3	92.2	91.8	89.3
γ	120.8	120.6	120.6	118.7	119.3	121.1	120.8	120.9
energy	0	0.314	0.490	0.674	1.012	0.908	1.313	0.976
d(003)	7.43	7.49	7.54	7.50	7.63	7.45	7.19	7.52

Numbers indicate the number of Al cations in each LDH layer. The 2-2-2 one is the original structure optimized. Energy is the energy difference (in eV) per unit cell with respect to the lowest energy arrangement. Distances are in Å, and angles in °.

Table 6

Intralayer Al^{3+} cation ordering in the 2-2-2 interlayer arrangement of 4x6x1 supercells of Mg-LDH and Zn-LDH optimized with CASTEP (E cut-off = 489.8 eV).

Parameters ordering	Mg-LDH			Zn-LDH		
	MaxD	MinD	L	MaxD	MinD	L
a	3.058	3.056	3.055	3.128	3.127	3.126
b	3.048	3.045	3.043	3.106	3.100	3.093
c	22.472	22.530	22.490	22.431	22.464	22.441
α	89.6	90.0	90.0	89.4	89.8	89.8
β	90.0	90.1	89.9	90.0	89.9	90.1
γ	120.4	120.3	120.2	120.8	120.4	120.3
energy	0	0.132	0.094	0	0.087	0.081

MaxD is the original structure optimized and discussed in the previous section. MinD refers to the structure with all cations bound together and L refers to the structure with all cations in line. Energy is the difference per unit cell with respect to the lowest energy configuration. All the distances are in Å, angles in ° and energy in eV.

systems, Mg-LDH and Zn-LDH with similar energy differences between the interlayer cation ordering arrangements.

On the other hand, within this interlayer cation ordering, we have to consider also the anion ordering, because of some changes in this ordering can alter the charge balance within the interlayer space. In the most stable cation arrangement, 2-2-2, the anion distribution is also ordered 2-2-2, that we can name A222 to distinguished from the cation ordering nomenclature. In the cation arrangement 2-3-1 the A222 anion distribution is also the most stable. Nevertheless, we calculated the A231 distribution and it was 0.195 eV/unit-cell less stable than A222. In the 1-4-1 model the A222 configuration is not the most stable one. The A231 is 0.337 eV/unit-cell more stable than A222, because in the …1-4-1-1-4-1… interlayer cation sequence more anions have to be closer to the layer with more Al cations for change compensation (Table 4). However, the A141 is less stable (0.307 eV/unit-cell) than A222 because it produces a deformation in the cationic layer due to the high negative charge in the interlayer. For the 3-0-3 model, the A312 has higher energy than A303 (0.296 eV/unit-cell). However, the A303 configuration seems to be the least probable, due to the high deformation observed in the structure. In the A303 configuration, the cationic layers above and below the chlorine-free interlayer are very close, resulting in the deformation of the OHs in the layer without aluminium cations (see Fig. S4). Similar behaviours have been observed in Zn-LDH structures (Table 5). Therefore, we can conclude that for cation distributions 2-2-2 and 2-3-1, the most stable anion configuration is the A222; while for cation distributions 1-4-1 and 3-0-3, the most stable anion configurations are those in which the anions are distributed according to balance the charges, without acquiring the arrangements of the cations, i.e. A231 and A312, respectively.

Taking into account that the ordered 2-2-2 interlayer distributions are the energetically most favourable for Mg-LDH and Zn-LDH, the intralayer arrangement of the aluminium atoms within the cationic layers has been also studied in the central layer of both Mg-LDH and Zn-LDH 2-2-2 structures. Three different intralayer arrangements of Al cations were considered in the second cationic layer (Fig. 2): MaxD, MinD, and L shape. After the optimization, all structures have almost the same lattice parameters as the original structure (Table 6). However, the energy of the structures is different, being the lowest energy the original ordered structure (i.e. 2-2-2 structure) with maximal intralayer Al dispersion and the one with highest energy is the structure with minimum dispersion of the Al^{3+} cations.

These energy differences of intralayer ordering are smaller than the above interlayer ordering. This indicates that the maximal dispersion of Al^{3+} cations is the most probable ordering in both senses, interlayer and intralayer ordering. Nevertheless, the experimental synthetic preparation processes of samples are at room or higher temperatures in fast reactions where a certain proportion of some of the above energetically

disfavoured cation arrangements can be formed in both systems. In contrast to synthetic LDH, Krivovichev et al. (2010) reported a crystallographic analysis of several natural LDH crystals considering both 2D (intralayer) and 3D (interlayer) ordering finding a natural tendency to form ordered 2D and 3D superstructures in the sulfates and carbonates LDH with M^{2+}-M^{3+} ratio of 2:1. Previous experimental studies have observed a cation ordering phenomenon during the aging of the Mg-LDH with Mg:Al 2:1 ratio by a dissolution-recrystallization process (Richardson and Braterman, 2007), confirming our discussion. Nevertheless, previous experimental studies of LDH with Mg:M 2:1 ratio have demonstrated that trivalent M^{3+} cations are completely scattered, in the octahedral layers of Mg:Fe LDH by X-ray absorption (EXAFS) (Vucelic et al., 1997) and of Mg:Al LDH by Nuclear Magnetic Resonance (NMR) (Sideris et al., 2008; Cadars et al., 2011) studies.
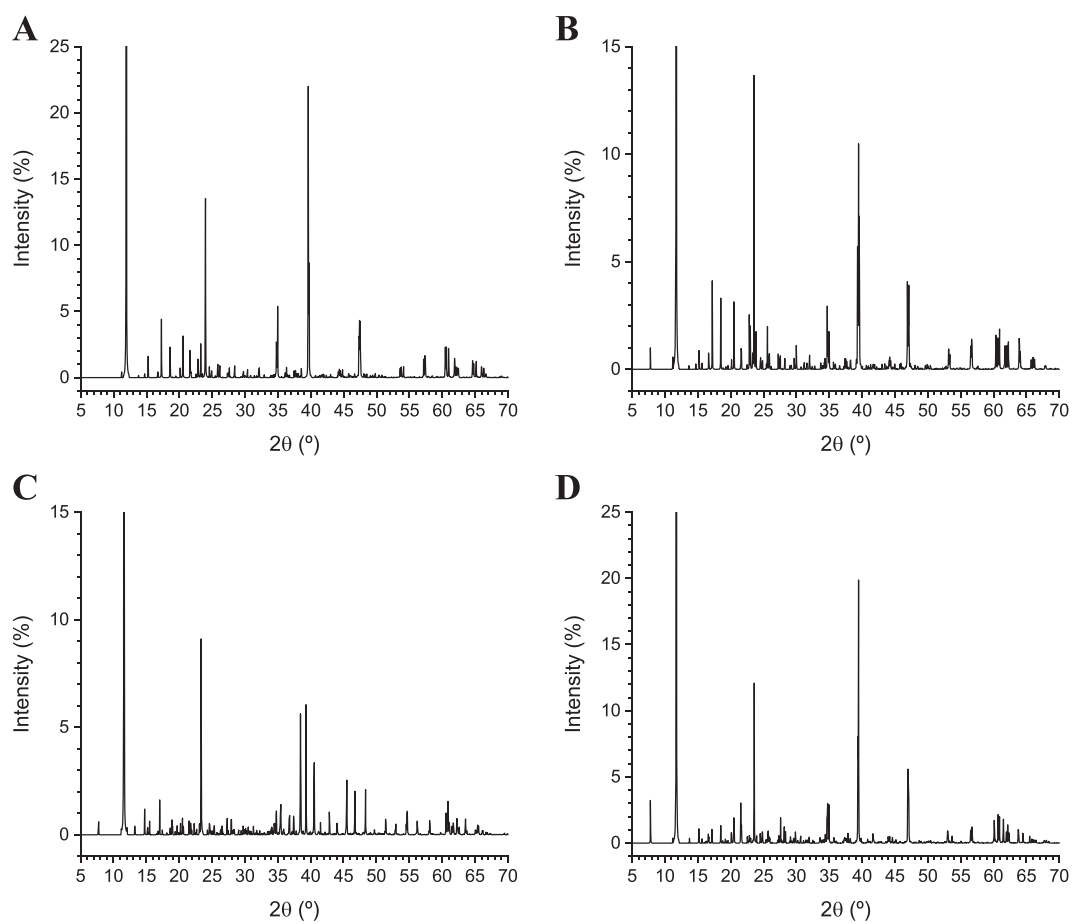
4.3. Diffractograms

After optimizing all structures with the different cation arrangements, diffractograms for each structure were simulated without imposing any symmetry restriction. Therefore, small diffraction peaks can appear due to changes in the crystal lattice. Nevertheless, some of these peaks of low intensity would not appear by imposing its original $R\bar{3}m$ crystal system, due to the limitation of our models where only short range ordering is studied.

In all diffractograms, the main peaks appear in the region of 10–15° for (003) reflection, 20–25° for (006), ~35° for (012), ~40° for (015) and 45–50° for (018) (Figs. 6–8), which are in good agreement with the experimental diffractograms previously reported (Cavani et al., 1991; Leroux et al., 2001; Forano et al., 2006; Pisson et al., 2008; Andre et al., 2015). In the case of structures with different numbers of Al^{3+} cations per layer, a detailed analysis makes it possible to distinguish the different structures. Thus, in the case of Mg-LDH, the different positions and shapes of the peaks corresponding to (006), (015) and (018) reflections could allow to differentiate between the different cation arrangements (Figs. 6 and 7). The non-ordered arrangements produce an additional reflection at 8° that is not observed in the 2-2-2 one (Fig. 6). This low angle reflexion comes from the higher space planes along the *c* axis as a consequence of the interlayer disorder, being as lower angle as the highest is the asymmetry coming from the interlayer disorder. This fact is interesting for interpreting experimental XRD analysis in these LDH. For instance, in the diffractogram reported by Andre et al. (2015), the author interpreted as an artefact one peak close to 8°. However, we have discovered that it could not be an artefact and it can be the 002 reflection produced by the different non-ordered arrangement of the Al^{3+} cations in the cationic layers. This peak has a certain intensity in the 3-0-3 configuration. It is interesting to note that this 002 peak has not been observed in other theoretical studies on LDH in which only one layer and one intralayer have been used (Costa et al., 2011), supporting the goodness of the results obtained in this work.

On the other hand, the presence of multiple peaks at 35°, 40° and 47° zones in disordered arrangements, like 4-1-4 (Fig. 6c) is consistent with the broad peaks observed experimentally in these zones in LDH synthesized (Boclair et al., 2001; Frost et al., 2009).

In the intralayer ordering configurations (Fig. 7A and B), only differences in relative intensity are observed. The MinD and L arrangements show reflections at <10° that do not appear in MaxD. Probably they are related with the cation ordering. Nevertheless, their relative intensities are too small (< 1%) to be considered.

For Zn-LDH structures, the peaks that could allow to distinguish between the different cation arrangements are those belonging to (012), (015) and (018) reflections (Figs. 7C, D and 8). In addition, it could be also possible to identify a peak close to ~8° in the 1-4-1 and 3-0-3 structures, and very small in the 2-3-1, which belongs to the (002) plane, and comes from the larger space due to the interlayer disorder. In this Zn-LDH case, the effect of distortions coming from the interlayer disorder
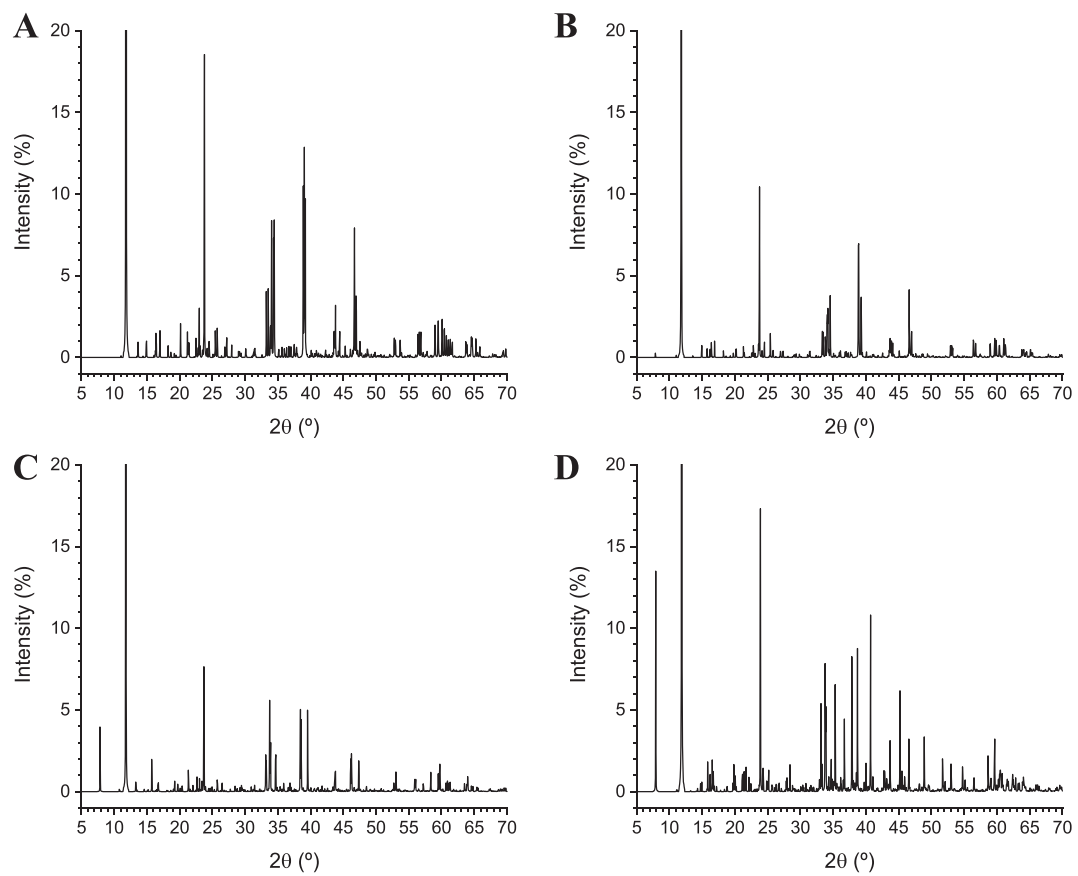
Fig. 6. XRD diffractograms of the interlayer cation arrangements of Mg-LDH, 2-2-2 (A), 2-3-1 (B), 1-4-1 (C), and 3-0-3 (D). All diffractograms have been truncated to allow better visualisation of the less intense peaks, being the peak (003), ~12° the most intense one with 100%. This is extended to the rest of diffractograms below.
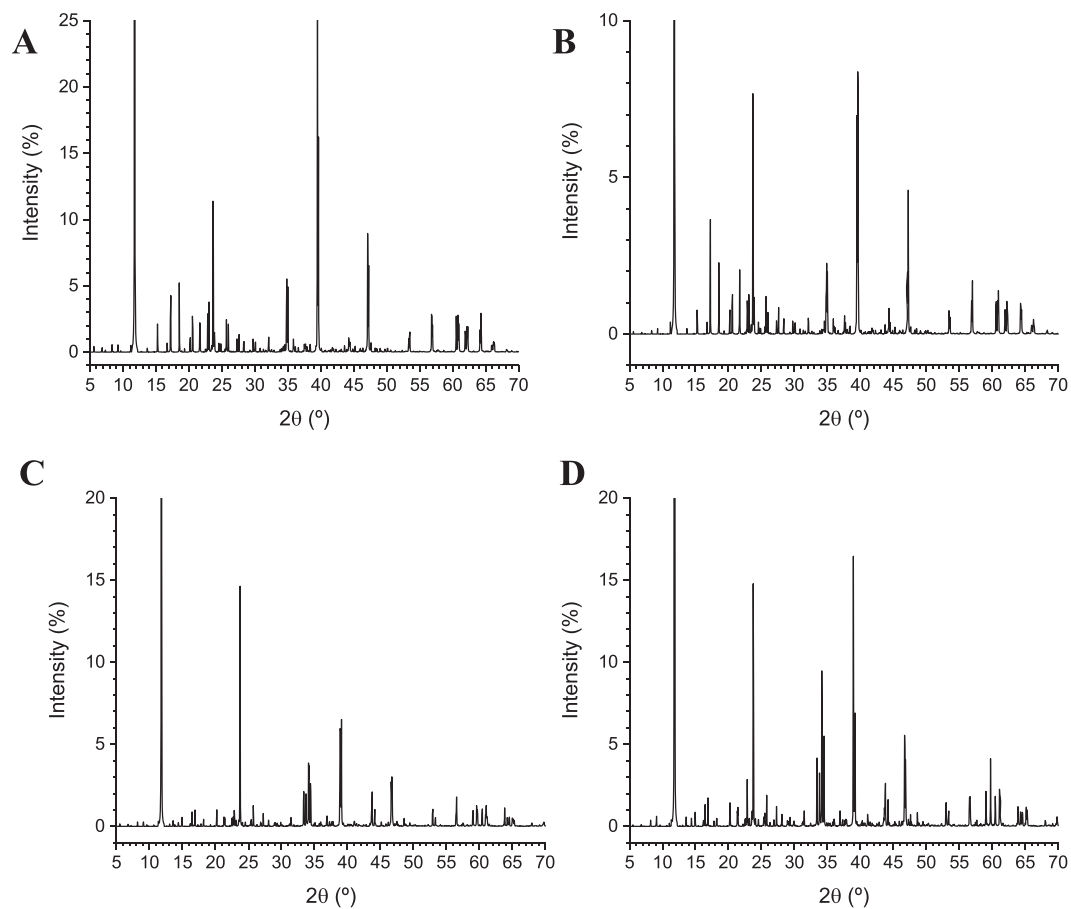
Fig. 7. XRD diffractograms of the intralayer cation arrangements of Mg-LDH and Zn-LDH. Mg-LDH diffractograms for the different cation arrangements are: MaxD (see Fig. 6A), MinD (A), and form L (B). For Zn-LDH the diffractograms correspond to MaxD (see Fig. 8a), MinD (C), and form L (D).

Fig. 8. XRD diffractograms of the interlayer cation arrangements of Zn-LDH, 2-2-2 (A), 2-3-1 (B), 1-4-1 (C), and 3-0-3 (D).

is much more intense in the 3-0-3 arrangement. In contrast to the diffractograms obtained for Mg-LDH, the Zn-LDH (002) reflection has a higher intensity, up to 14%, due to the high scattering factor difference between Zn and Al.

In the intralayer ordering configurations no clear differences were observed, being only in some relative intensities that we cannot related with the cation ordering differences with the available data (Fig. 7C and D).

4.4. Vibrational properties

In many minerals the IR spectroscopy has been useful for obtaining some insights into cation ordering (Cuadros et al., 1999; Sainz-Díaz et al., 2000, 2001, 2002; Timón et al., 2003; Botella et al., 2004; Ortega-Castro et al., 2009), but there have been only a few attempts to probe this structural property in LDHs. In these minerals, each hydroxyl group is coordinated to three cations. Then, the frequencies of the vibration modes of these groups will depend on the nature of the cations joined to it. Besides, these frequencies and intensities can depend also on additional interactions of these hydroxy groups with their local environment, second neighbour cations, interlayer anions and water molecules (Hernández-Haro et al., 2014). Costa et al. (2010) reported DFT calculations of infrared frequencies of the OH and CO_3 vibration modes of the ordered cation configuration carbonates of Mg_Al_LDH and Zn_Al_LDH and Zn_Al_Cl_LDH. Hence, we have calculated the frequencies of the main normal modes of these hydroxy groups in our LDH samples at

Table 7
Calculated frequencies (in cm^{-1}) of the main IR vibration modes of the structures of Mg-LDH with several cation orderings calculated with CASTEP and QE (in brackets).

modes	Exp.[a]	MgAl[b] 2-2-2	MgAl[b] 1-4-1	MgAl[b] 3-0-3	MgAl[b] 2-3-1
ν(OH) (MgMgMg)	3800–3680, 3770[c], 3698[d], 3650[e]	3684–3610 (3606, 3548)	3865–3827; 3813–3799; 3725–3691	3887–3840	3843–3827; 3776–3725; 3531
ν(OH) (MgAlMg)		3607–3472 (3796–3793, 3669–3495, 3446–3397)	3821–3816; 3781–3731; 3653–3346	3752; 3609–3539; 3328–3206; 3136–3085	3804–3789; 3718–3629; 3531–3399; 3346; 3305–3082
ν(OH) (AlMgAl)		3466–3416 (3470–3453, 3366–3060)	3254–3139; 3008–2409	3710–3701; 3464–3364; 3168; 2972–2789	3367; 3346; 3324; 3014–2875
ν(OH) (AlAlAl)			3068; 2182		
δ(OH) (AlMgAl)		1005–993; 890; 821 (921, 867–860, 730)	1144–1048; 1016–1008; 964; 938; 919; 821; 786;	1121–1096; 1008–965	1056–1008; 930–903;
δ(OH) (MgAlMg)		982–896; 884–827; 700 (1037–925, 901–898, 834–756, 737, 722)	988–972; 939; 926; 889–859; 808–800; 784–782; 761–755; 742;	1031–1018; 898–706	999–934; 897–814; 745; 729–719
δ(OH) (MgMgMg)	703	816–733 (805, 749)	777; 746; 727–708;	699–690	753–749; 736
δ(OH) (AlAlAl)			1032; 900; 704;		

[a] Experimental data from brucite (Braterman and Cygan, 2006).
[b] Cation arrangement, the numbers indicate the number of Al in each layer per supercell.
[c] Experimental values from brucite (Chakoumakos et al., 1997).
[d] Experimental values from Lutz et al. (1994).
[e] Experimental values from de Oliveira and Hase (2001).

Table 8
Calculated frequencies (in cm^{-1}) of the main IR vibration modes of the calculated 2-2-2 structures of Mg-LDH with water and Zn-LDH.

Modes[a]	Exp.[b]	MgAl water	ZnAl	ZnAl water
ν(OH) (MMM)	3800–3680, 3770[c], 3698[d], 3650[e]	3755–3729; 3648; 3615; 3552 (3597, 3548)	3625–3603; 3506 (3640)	(3571, 3309)
ν(OH) (MAlM)	(3588, 3439)[f]	3685–3654; 3587–3572; 3517–3501; 3452–3449; 3442; 3383; 3356 (3671–3627, 3611, 3602, 3590, 3579–3554, 3416, 3394, 3362)	3531–3517; 3502–3409 (3756–3736, 3625–3535, 3474–3439, 3384–3199)	(3661–3605, 3598, 3456, 3380, 3370)
ν(OH) (AlMAl)		3642; 3445; 3429; 3371; 3317 (3464, 3337)	3640 (3500–3488, 3431)	(3409, 3282)
ν(OH) (H_2O)		3624; 3561; 3531; 3471–3456; 3444; 3330; 3299–3100 (3627, 3602, 3597, 3590, 3579–3556, 3554–3548, 3540, 3464, 3396, 3250, 3218, 3163, 3053, 2955)		(3604–3600, 3584, 3444, 3260–3127)
δ(OH)[g] (H_2O)	1635[f]	1655–1558 (1642–1562)		(1644, 1618–1516)
δ(OH) (AlMAl)		1101; 1008; 885 (1116, 1024–877, 924–675)	1003; 989 (1061, 1010–1002, 970–692)	(1088, 1044–606)
δ(OH) (MAlM)	854[f]	1093–1022; 976–900; 873–856; 814; 786; 765–728; 718; 706 (1116–1110, 1024–877, 924–675)	1008; 995; 982–879; 867–849; 811–702 (1011, 994, 971)	(1044–606)
δ(OH) (MMM)	703, 733[f]	829; 812–809; 785–783;	871; 838–817 (803, 772)	(1044–606)
γ(OH) (H_2O)		778–774; 726; 709 (1024–877, 924–675)		(1044–606)

Values from CASTEP calculations. Values in brackets are calculated with QE.
[a] M means Mg or Zn.
[b] Experimental data from brucite (Braterman and Cygan, 2006).
[c] Experimental values from brucite (Chakoumakos et al., 1997).
[d] Experimental values from Lutz et al. (1994).
[e] Experimental values from de Oliveira and Hase (2001).
[f] Experimental values (Frost et al., 2009).
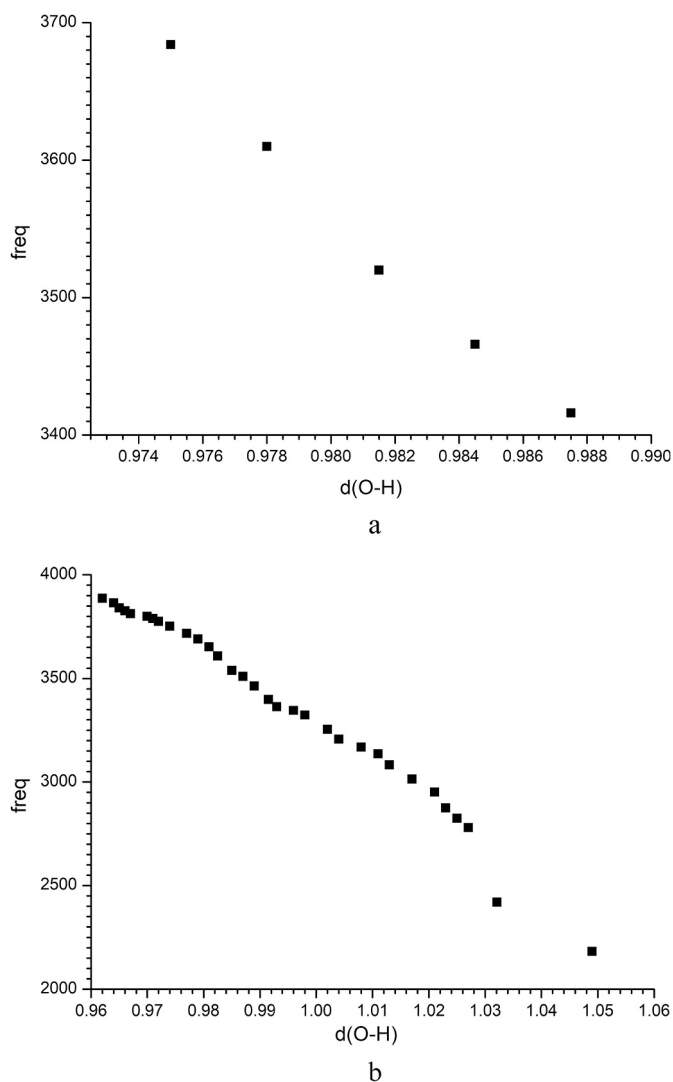[g] Scissors bending vibration.

a

b

Fig. 9. Relationship between d(OH) bond lengths (in Å), figure a, and the ν(OH) frequencies (in cm^{-1}), figure b, of Mg-LDH.

quantum mechanical level.

In the dispersed cation arrangements, no OH joined to AlAlAl group is observed, but only in the 1-4-1 arrangement, due to the high Al content in one layer. The ν(OH) frequencies change with the nature of the cations which are joined with, following the sequence: MgMgMg > MgAlMg > AlMgAl > AlAlAl. Within the same type of cation ensemble, the frequencies changes depending on the local environment of each OH group yielding a range of frequencies where similar OH groups vibrate coupled each other. In some cases, the effect of the local environment is stronger than the effect of the nature of cations which are joined with (Tables 7 and 8). In the samples with different cation arrangements the number of Al^{3+} cations per layer is directly related with the number of chloride anions in the interlayers. Hence, the OH groups in layers with low Al content will have less interlayer anions and less H bonds or electrostatic interactions and the frequencies will be higher than in other OH groups with more interactions with anions. Extremely low frequency values are observed in the ordering pattern 1-4-1 of MgAl where ν(OH) (AlMgAl) appears at 2409 cm^{-1} due to a strong H bond between the OH group and the Cl$^-$ anion with d(O—H) = 1.043 Å, and d(Cl...HO) = 1.845 Å. In the AlAlAl OH group of this 1-4-1 cation arrangement, ν(OH) appears at 2182 cm^{-1} due to a dissociation process of the OH group with d(O—H) = 1.650 Å, and d(Cl...HO) = 1.342 Å, where there is a high charge concentration.

In the disordered 2-3-1, 1-4-1 and 3-0-3 configurations, the whole range of ν(OH) is 3887–2182 cm^{-1} wider than in the 2-2-2 one 3684–3416 cm^{-1} (Table 7). This is consistent with the broad band observed experimentally in the range of 3850–3000 cm^{-1}, where bands corresponding to water molecules are also included (Richardson and Braterman, 2007). We found similar frequencies for the water ν(OH) bands in the range 3624–3100 cm^{-1} (Table 8). However, Richardson and Braterman (2007) observed that this broad band changed to a more narrow profile during the aging process of the Mg-LDH, suggesting a cation ordering process during the aging. Our results confirm this hypothesis, where the initial stage of the synthetic Mg-LDH would be a mixture of many disordered cation arrangements including the 2-2-2, 2-3-1, 1-4-1, and 3-0-3. During the aging process, these configurations would transform to a more ordered cation distribution like the 2-2-2 model, explaining the reduction of the width of the IR ν(OH) band with the aging time observed experimentally. The absence of the ν(OH) (AlAlAl) in the 2-2-2 ordered configuration is consistent with previous experimental NMR data of Mg$_2$Al LDH (Cadars et al., 2011).

We have calculated the radial distribution function of the O—H bonds for the cation arrangements of Mg-LDH (Fig. S5) and Zn-LDH (Fig. S6). Some differences were observed, where the profile of these O—H distances changes with the cation ordering. In the ordered 2-2-2 configuration, the d(O—H) bond length is within a narrow range (0.974–0.988 Å), whereas the disordered configurations the range of d (O—H) is wider (0.96–1.05 Å). Similar behaviour was found in Zn-LDH configurations. These differences in the O—H bond are directly related with the differences in the ν(OH) frequencies. We can correlate the d (O—H) bond length with the ν(OH) frequency of the ordered 2-2-2 structure observing a linear relationship decreasing the frequencies when the d(O—H) increases (Fig. 9a). Besides, considering the d(O—H) bond lengths of all disordered structures and their ν(OH) frequencies we can find a similar linear relationship (Fig. 9b).

On the other hand, the radial distribution function of the non-bonding OH....Cl distances was also calculated (Figs. S7 and S8). The profiles of these distances also change with the cation ordering. In the ordered 2-2-2 cation arrangement, the range of this distance (2.17–2.5 Å) is narrower than in the disordered models. In the disordered models the d(H...Cl) distances can be lower than 1.9 Å, especially 1-4-1 that can be at 1.85 Å (in Mg-LDH) and 1.94 Å (in Zn-LDH), due to the charge concentration in some zones of the crystal lattice producing a higher electrostatic attraction. This indicates that the interactions of the chloride anions on the OH H atoms are the main responsible of the d(OH) variations.

In the bending δ(OH) vibration mode, the frequencies also vary with the nature of the cations which are joined with, following the sequence: MgMgMg < MgAlMg < AlMgAl < AlAlAl. This sequence is the opposite to that of ν(OH). A similar sequence was observed previously in dioctahedral 2:1 phyllosilicates where MgMg < AlMg < AlAl in this vibration mode (Escamilla-Roa et al., 2014; Hernández-Haro et al., 2014). Nevertheless, the local environment of each OH can also alter the δ(OH) frequency and overlap the above sequence. In general, the δ(OH) vibrations of most OH groups are coupled and most are combination vibrations of several OH groups. Nevertheless, their frequency ranges of δ(OH) are consistent with previous experimental studies (Andre et al., 2015).

Small differences are found between the frequency values calculated with CASTEP and QE. The MgAlMg ν(OH) frequencies are larger with QE than with CASTEP, whereas the MgMgMg ν(OH) frequencies are smaller in QE than with CASTEP. However, these differences are within the overlapping and coupling of the ν(OH) vibration modes of all OH groups. The same is observed in the δ(OH) frequencies.

In the hydrated samples the ν(OH) frequencies of water molecules appear in the same frequency range as the others OH groups and many are coupling each other (Table 8). When the water H atoms are oriented and close to the Cl anions, their ν(OH) frequencies decrease reaching a vey low frequencies, lower than 3000 cm^{-1}, similar results were found
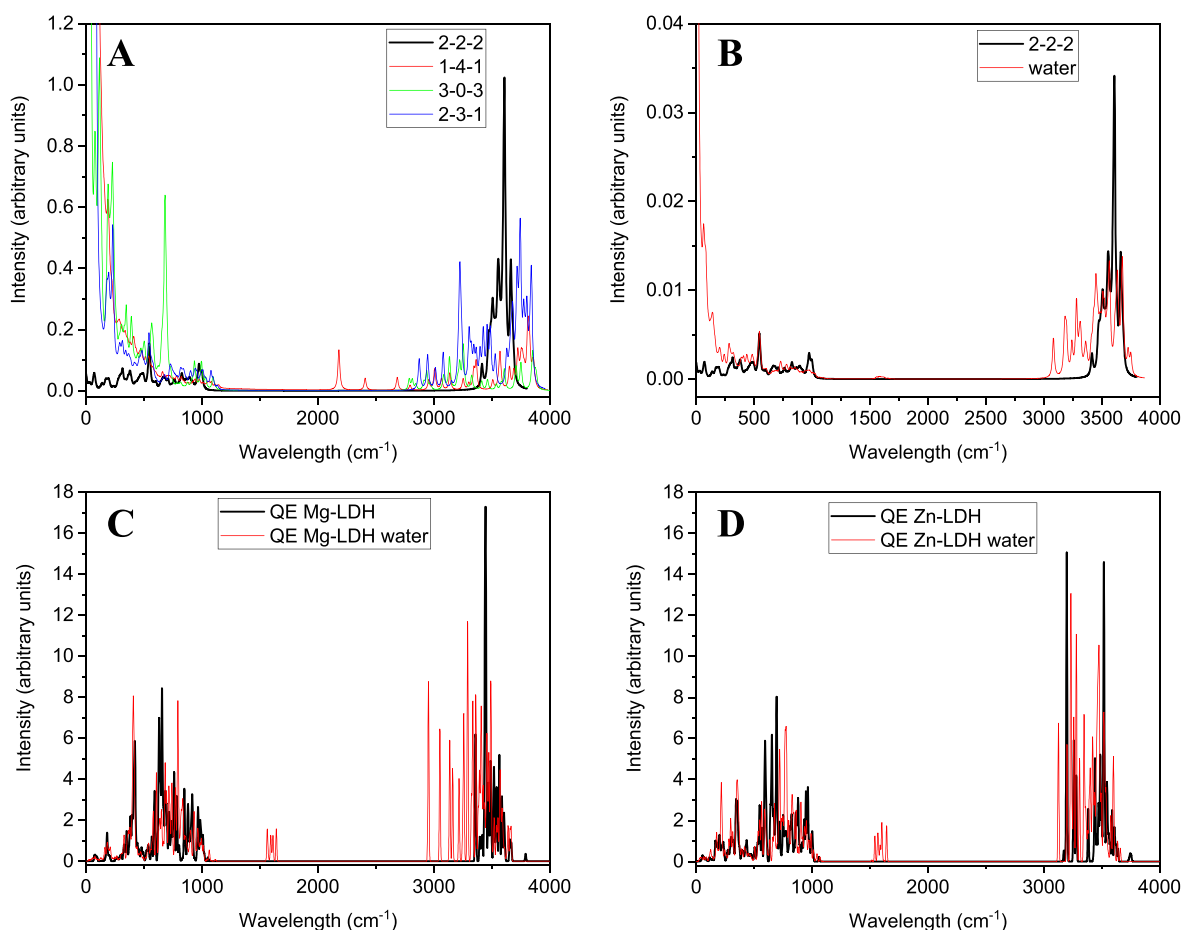
Fig. 10. Raman spectra of LDH. A) Raman spectra simulated using CASTEP for Mg-LDH with different Al^{3+} cations arrangements per layer. B) CASTEP Raman spectra of anhydrous and hydrated Mg-LDH. C) Raman spectra simulated using QE for anhydrous and hydrated Mg-LDH. D) Raman spectra simulated using QE for anhydrous and hydrated Zn-LDH.

by Costa et al. (Costa et al., 2010) calculations. Nevertheless, in general, the $\nu(OH)$ frequencies of the structural OH groups are smaller than in the dry samples, due to the H bonding interactions between the hydroxyl H atoms and the water O atoms. The $\nu(OH)$ frequencies of water in these hydrated systems are in the similar range than the $\nu(OH)$ of MOHM' groups. Hence, the classical assignments of the lower $\nu(OH)$ frequencies for water and the higher ones for the MOHM' groups should be revisited (Kloprogge et al., 2004; Frost et al., 2009).

In the ZnAl samples, in general, the $\nu(OH)$ frequencies are slightly lower than in MgAl samples (Table 8) and follow a similar sequence ZnZnZn > ZnAlZn > AlZnAl that in Mg-LDH models. In $\delta(OH)$ the frequencies follow the opposite sequence as in Mg, AlZnAl > ZnAlZn > ZnZnZn. In these solids similar differences between the frequency values calculated with CASTEP and with QE are found to those in Mg-LDH. The $\delta(OH)$ of the confined water molecules at 1644 cm^{-1} are consistent with previous experimental values at 1631 cm^{-1} (Mahjoubi et al., 2017).

Raman spectra for LDH structures had also been calculated using both CASTEP and QE (Fig. 10). The Raman spectrum of Mg-LDH with 2 Al^{3+} cations per layer (2−2−2) is close to the experimental Mg-LDH reported by Andre et al. (2015). In such paper, authors reported a Raman spectrum between 200 and 1200 cm^{-1}, having the highest intensity close to 550 cm^{-1} and the second highest intensity close to 1000 cm^{-1}. In the Mg-LDH Raman spectrum, two peaks close to 550 and 1000 cm^{-1} are the highest and the second highest peaks in the region between 200 and 1200 cm^{-1}. This results with CASTEP seem to be more similar to the experimental ones that those theoretical results reported previously (Andre et al., 2015). The peak close to 550 cm^{-1} appears also in hydrated Mg-LDH and in the Mg-LDH with different Al^{3+} cation

arrangement per layer (Fig. 11A). Notice, the differences observed in the Raman spectra with different cation arrangement. This indicates that this analytical technique can be very useful for detecting cation ordering stages in LDH. Slight differences are observed in the frequencies and relative intensities calculated with QE.

5. Conclusions

In this work, we show that atomistic DFT calculations of cation ordering of M-LDH can be a useful approach for understanding and characterizing this phenomenon experimentally. The calculated parameters setups at quantum mechanical level have been validated, reproducing the crystal lattice structure of LDH. In both systems, MgAl 2:1- and ZnAl 2:1-LDH, the maximal dispersion of the trivalent cations is the most favourable energetically. However, the energy differences are not very high, indicating that synthetic conditions can alter the crystallization process and some changes in cation ordering can be produced by kinetic control at room or higher temperatures. This can justify the fact that the natural LDH have a higher cation ordering generally than in synthetic LDH samples probably due to the rate of formation and aging process of the natural minerals producing changes in the layers stacking and the relative position of cations.

Simulated diffractograms are in good agreement with previously reported experimental diffractograms. In addition, the different arrangement of the Al^{3+} cations could be identified in the diffractograms by the presence of new peaks, as discussed in this paper regarding a previous work in which these peaks were misinterpreted as an artefact, such as the (002) peak. These results seem to be suitable for future

experimental work studying the cation ordering of LDH using diffraction techniques.

The calculated frequencies of the main vibration modes are consistent with experimental observations. The frequencies of the OH groups are highly dependent of the cations which are joined with and the interactions with the interlayer anions. These last interactions can be strong decreasing drastically the ν(OH) frequencies. Interesting changes in frequencies are observed with the cation ordering. Our calculations have found the justification of the profile changes in ν(OH) bands observed experimentally during the aging of synthetic Mg-LDH. This information can be useful for further investigations with experimental spectroscopic studies of LDH monitoring the cation ordering with synthetic conditions.

CRediT authorship contribution statement

Carlos Pimentel: Data curation, Formal Analysis, Investigation, Writing - original draft, Writing - review & editing. **Alexander Pérez de la Luz**: Data curation, Formal Analysis, Investigation, Writing - review & editing. **Alfonso Hernández-Laguna:** Writing – review & editing. C. **Ignacio Sainz-Díaz:** Conceptualization, Investigation, Supervision, Writing - original draft, Writing - review & editing

Declaration of Competing Interest

The authors declare that they have no known competing financial interests or personal relationships that could have appeared to influence the work reported in this paper.

Acknowledgements

Appendix A. Supplementary data

Supplementary data to this article can be found online at https://doi.org/10.1016/j.clay.2022.106496.

References

Allmann, R., Jepsen, H., 1969. Die struktur des hydrotalkits. Neues Jahrb. Für Mineral. Monatshefte 1969, 544–551.

Andre, E., Fahel, J., Carteret, C., 2015. Modelling the Structure and Vibrational Properties of Layered double Hydroxides. In: Energy Technology 2015. John Wiley & Sons, Ltd, pp. 317–323. https://doi.org/10.1002/9781119093220.ch35.

Baroni, S., Giannozzi, P., Testa, A., 1987. Green's-function approach to linear response in solids. Phys. Rev. Lett. 58, 1861–1864. https://doi.org/10.1103/PhysRevLett.58.1861.

Baroni, S., de Gironcoli, S., Dal Corso, A., Giannozzi, P., 2001. Phonons and related crystal properties from density-functional perturbation theory. Rev. Mod. Phys. 73, 515–562. https://doi.org/10.1103/RevModPhys.73.515.

Biovia, 2018. Materials Studio 2019. Dassault Systèmes, San Diego.

Blöchl, P.E., 1994. Projector augmented-wave method. Phys. Rev. B 50, 17953–17979. https://doi.org/10.1103/PhysRevB.50.17953.

Boclair, J.W., Braterman, P.S., Brister, B.D., Yarberry, F., 1999. Layer−anion interactions in magnesium aluminum layered double hydroxides intercalated with cobalticyanide and nitroprusside. Chem. Mater. 11, 2199–2204. https://doi.org/10.1021/cm990148l.

Boclair, J.W., Braterman, P.S., Brister, B.D., Wang, Z., Yarberry, F., 2001. Physical and chemical interactions between Mg:Al layered double hydroxide and

hexacyanoferrate. J. Solid State Chem. 161, 249–258. https://doi.org/10.1006/jssc.2001.9306.

Botella, V., Timón, V., Escamilla-Roa, E., Hernández-Laguna, A., Sainz-Díaz, C.I., 2004. Hydrogen bonding and vibrational properties of hydroxy groups in the crystal lattice of dioctahedral clay minerals by means of first principles calculations. Phys. Chem. Miner. 31, 475–486. https://doi.org/10.1007/s00269-004-0398-7.

Braterman, P.S., Cygan, R.T., 2006. Vibrational spectroscopy of brucite: a molecular simulation investigation. Am. Mineral. 91, 1188–1196. https://doi.org/10.2138/am.2006.2094.

Cadars, S., Layrac, G., Gérardin, C., Deschamps, M., Yates, J.R., Tichit, D., Massiot, D., 2011. Identification and quantification of defects in the cation ordering in Mg/Al layered double hydroxides. Chem. Mater. 23, 2821–2831. https://doi.org/10.1021/cm200029q.

Cavani, F., Trifirò, F., Vaccari, A., 1991. Hydrotalcite-type anionic clays: preparation, properties and applications. Catal. Today 11, 173–301. https://doi.org/10.1016/0920-5861(91)80068-K.

Chakoumakos, B.C., Loong, C.-K., Schultz, A.J., 1997. Low-temperature structure and dynamics of brucite. J. Phys. Chem. B 101, 9458–9462. https://doi.org/10.1021/jp972225a.

Clark, S.J., Segall, M.D., Pickard, C.J., Hasnip, P.J., Probert, M.I.J., Refson, K., Payne, M. C., 2005. First principles methods using CASTEP. Z. Für Krist. – Cryst. Mater. 220, 567–570. https://doi.org/10.1524/zkri.220.5.567.65075.

Costa, D.G., Rocha, A.B., Diniz, R., Souza, W.F., Chiaro, S.S.X., Leitão, A.A., 2010. Structural model proposition and thermodynamic and vibrational analysis of hydrotalcite-like compounds by DFT calculations. J. Phys. Chem. C 114, 14133–14140. https://doi.org/10.1021/jp1033646.

Costa, D.G., Rocha, A.B., Souza, W.F., Chiaro, S.S.X., Leitão, A.A., 2011. Ab initio simulation of changes in geometry, electronic structure, and gibbs free energy caused by dehydration of hydrotalcites containing Cl− and CO32− counteranions. J. Phys. Chem. B 115, 3531–3537. https://doi.org/10.1021/jp110668s.

Cuadros, J., Sainz-Diaz, C.I., Ramirez, R., Hernandez-Laguna, A., 1999. Analysis of Fe segregation in the octahedral sheet of bentonitic illite-smectite by means of FTIR, 27 Al MAS NMR and reverse Monte Carlo simulations. Am. J. Sci. 299, 289–308. https://doi.org/10.2475/ajs.299.4.289.

de Oliveira, E.F., Hase, Y., 2001. Infrared study and isotopic effect of magnesium hydroxide. Vib. Spectrosc. 25, 53–56. https://doi.org/10.1016/S0924-2031(00)00107-7.

Duval, S., Baymann, F., Schoepp-Cothenet, B., Trolard, F., Bourrié, G., Grauby, O., Branscomb, E., Russell, M.J., Nitschke, W., 2019. Fougerite: the not so simple progenitor of the first cells. Interface Focus 9, 20190063. https://doi.org/10.1098/rsfs.2019.0063.

Ennadi, A., Legrouri, A., De Roy, A., Besse, J.P., 2000. X-ray diffraction pattern simulation for thermally treated [Zn–Al–Cl] layered double hydroxide. J. Solid State Chem. 152, 568–572. https://doi.org/10.1006/jssc.2000.8740.

Escamilla-Roa, E., Hernández-Laguna, A., Sainz-Díaz, C.I., 2014. Theoretical study of the hydrogen bonding and infrared spectroscopy in the cis-vacant polymorph of dioctahedral 2:1 phyllosilicates. J. Mol. Model. 20, 2404. https://doi.org/10.1007/s00894-014-2404-4.

Evans, D.G., Slade, R.C.T., 2006. Structural aspects of layered double hydroxides. In: Duan, X., Evans, D.G. (Eds.), Layered Double Hydroxides, Structure and Bonding. Springer, Berlin, Heidelberg, pp. 1–87. https://doi.org/10.1007/430_005.

Figueiredo, M.P., Cunha, V.R.R., Leroux, F., Taviot-Gueho, C., Nakamae, M.N., Kang, Y. R., Souza, R.B., Ana Maria Martins, C.R.P.F., Koh, I.H.J., Constantino, V.R.L., 2018. Iron-based layered double hydroxide implants: potential drug delivery carriers with tissue biointegration promotion and blood microcirculation preservation. ACS Omega 3, 18263–18274. https://doi.org/10.1021/acsomega.8b02532.

Figueiredo, M.P., Duarte, A., Vendruscolo, V., Thirouard, R., Constantino, V.R.L., Taviot-Guého, C., 2021. Investigation about iron(III) incorporation into layered double hydroxides: compositional and structural properties of Mg2FeyAl(1−y)(OH)6-Cl and Zn2FeyAl(1−y)(OH)6-Cl. J. Alloys Compd. 886, 161184 https://doi.org/10.1016/j.jallcom.2021.161184.

Forano, C., Hibino, T., Leroux, F., Taviot-Guého, C., 2006. Chapter 13.1 layered double hydroxides. In: Bergaya, F., Theng, B.K.G., Lagaly, G. (Eds.), Developments in Clay Science. Elsevier, Handbook of Clay Science, pp. 1021–1095. https://doi.org/10.1016/S1572-4352(05)01039-1.

Frost, R.L., Spratt, H.J., Palmer, S.J., 2009. Infrared and near-infrared spectroscopic study of synthetic hydrotalcites with variable divalent/trivalent cationic ratios. Spectrochim. Acta A Mol. Biomol. Spectrosc. 72, 984–988. https://doi.org/10.1016/j.saa.2008.12.018.

Giannozzi, P., Baroni, S., Bonini, N., Calandra, M., Car, R., Cavazzoni, C., Ceresoli, D., Chiarotti, G.L., Cococcioni, M., Dabo, I., Corso, A.D., de Gironcoli, S., Fabris, S., Fratesi, G., Gebauer, R., Gerstmann, U., Gougoussis, C., Kokalj, A., Lazzeri, M., Martin-Samos, L., Marzari, N., Mauri, F., Mazzarello, R., Paolini, S., Pasquarello, A., Paulatto, L., Sbraccia, C., Scandolo, S., Sclauzero, G., Seitsonen, A.P., Smogunov, A., Umari, P., Wentzcovitch, R.M., 2009. QUANTUM ESPRESSO: a modular and open-source software project for quantum simulations of materials. J. Phys. Condens. Matter 21, 395502. https://doi.org/10.1088/0953-8984/21/39/395502.

Giannozzi, P., Andreussi, O., Brumme, T., Bunau, O., Nardelli, M.B., Calandra, M., Car, R., Cavazzoni, C., Ceresoli, D., Cococcioni, M., Colonna, N., Carnimeo, I., Corso, A.D., de Gironcoli, S., Delugas, P., DiStasio, R.A., Ferretti, A., Floris, A., Fratesi, G., Fugallo, G., Gebauer, R., Gerstmann, U., Giustino, F., Gorni, T., Jia, J., Kawamura, M., Ko, H.-Y., Kokalj, A., Küçükbenli, E., Lazzeri, M., Marsili, M., Marzari, N., Mauri, F., Nguyen, N.L., Nguyen, H.-V., Otero-de-la-Roza, A., Paulatto, L., Poncé, S., Rocca, D., Sabatini, R., Santra, B., Schlipf, M., Seitsonen, A.P., Smogunov, A., Timrov, I., Thonhauser, T., Umari, P., Vast, N., Wu, X., Baroni, S.,

2017. Advanced capabilities for materials modelling with Quantum ESPRESSO. J. Phys. Condens. Matter 29, 465901. https://doi.org/10.1088/1361-648X/aa8f79.

Greenwell, H.C., Coveney, P.V., 2006. Layered double hydroxide minerals as possible prebiotic information storage and transfer compounds. Orig. Life Evol. Biosph. 36, 13–37. https://doi.org/10.1007/s11084-005-2068-2.

Grimme, S., 2006. Semiempirical GGA-type density functional constructed with a long-range dispersion correction. J. Comput. Chem. 27, 1787–1799. https://doi.org/10.1002/jcc.20495.

Grimme, S., Antony, J., Ehrlich, S., Krieg, H., 2010. A consistent and accurate ab initio parametrization of density functional dispersion correction (DFT-D) for the 94 elements H-Pu. J. Chem. Phys. 132, 154104 https://doi.org/10.1063/1.3382344.

Hammouda, T., Andrault, D., Koga, K., Katsura, T., Martin, A.M., 2011. Ordering in double carbonates and implications for processes at subduction zones. Contrib. Mineral. Petrol. 161, 439–450. https://doi.org/10.1007/s00410-010-0541-z.

Hernández-Haro, N., Ortega-Castro, J., Pruneda, M., Sainz-Díaz, C.I., Hernández-Laguna, A., 2014. Theoretical study on the influence of the Mg2+ and Al3+ octahedral cations on the vibrational spectra of the hydroxy groups of dioctahedral 2:1 phyllosilicate models. J. Mol. Model. 20, 2402. https://doi.org/10.1007/s00894-014-2402-6.

Hofmeister, W., Platen, H.V., 1992. Crystal chemistry and atomic order in brucite-related double-layer structures. Crystallogr. Rev. 3, 3–26. https://doi.org/10.1080/08893119208032964.

Jayanthi, K., Kamath, P.V., Periyasamy, G., 2017. Electronic-structure calculations of cation-ordered II-III layered double hydroxides: origin of the distortion of the metal-coordination symmetry. Eur. J. Inorg. Chem. 2017, 3675–3682. https://doi.org/10.1002/ejic.201700716.

Kloprogge, J.T., Hickey, L., Frost, R.L., 2004. The effects of synthesis pH and hydrothermal treatment on the formation of zinc aluminum hydrotalcites. J. Solid State Chem. 177, 4047–4057. https://doi.org/10.1016/j.jssc.2004.07.010.

Kokalj, A., 1999. XCrySDen—a new program for displaying crystalline structures and electron densities. J. Mol. Graph. Model. 17, 176–179. https://doi.org/10.1016/S1093-3263(99)00028-5.

Krivovichev, S.V., Yakovenchuk, V.N., Zolotarev, A.A., Ivanyuk, G.N., Pakhomovsky, Y. A., 2010. cation ordering and superstructures in natural layered double hydroxides. Chim. Int. J. Chem. 64, 730–735. https://doi.org/10.2533/chimia.2010.730.

Kruissink, E.C., van Reijen, L.L., Ross, J.R.H., 1981. Coprecipitated nickel–alumina catalysts for methanation at high temperature. Part 1.—Chemical composition and structure of the precipitates. J. Chem. Soc. Faraday Trans. 1 Phys. Chem. Condens. Phases 77, 649–663. https://doi.org/10.1039/F19817700649.

Leroux, F., Adachi-Pagano, M., Intissar, M., Chauvière, S., Forano, C., Besse, J.-P., 2001. Delamination and restacking of layered doublehydroxides. J. Mater. Chem. 11, 105–112. https://doi.org/10.1039/B002955F.

Li, C., Zhao, S., Yao, X., He, L., Xu, S., Shen, X., Yao, Z., 2021. The catalytic mechanism of intercalated chlorine anions as active basic sites in MgAl-layered double hydroxide for carbonyl sulfide hydrolysis. Environ. Sci. Pollut. Res. https://doi.org/10.1007/s11356-021-16204-3.

Liu, H.-M., Zhao, X.-J., Zhu, Y.-Q., Yan, H., 2020. DFT study on MgAl-layered double hydroxides with different interlayer anions: structure, anion exchange, host–guest interaction and basic sites. Phys. Chem. Chem. Phys. 22, 2521–2529. https://doi.org/10.1039/C9CP05529K.

Lombardo, G.M., Pappalardo, G.C., Punzo, F., Costantino, F., Costantino, U., Sisani, M., 2005. A novel integrated X-ray Powder Diffraction (XRPD) and Molecular Dynamics (MD) Approach for Modelling Mixed-Metal (Zn, Al) Layered Double Hydroxides (LDHs). Eur. J. Inorg. Chem. 2005, 5026–5034. https://doi.org/10.1002/ejic.200500666.

Lombardo, G.M., Pappalardo, G.C., Costantino, F., Costantino, U., Sisani, M., 2008. Thermal effects on mixed metal (Zn/Al) layered double hydroxides: direct modeling of the X-ray powder diffraction line shape through molecular dynamics simulations. Chem. Mater. 20, 5585–5592. https://doi.org/10.1021/cm801053d.

Lutz, H.D., Möller, H., Schmidt, M., 1994. Lattice vibration spectra. Part LXXXII. Brucite-type hydroxides M(OH)2 (M = Ca, Mn, Co, Fe, Cd) — IR and Raman spectra, neutron diffraction of Fe(OH)2. J. Mol. Struct. 328, 121–132. https://doi.org/10.1016/0022-2860(94)08355-X.

Mahjoubi, F.Z., Khalidi, A., Abdennouri, M., Barka, N., 2017. Zn–Al layered double hydroxides intercalated with carbonate, nitrate, chloride and sulphate ions: Synthesis, characterisation and dye removal properties. J. Taibah Univ. Sci. 11, 90–100. https://doi.org/10.1016/j.jtusci.2015.10.007.

Mercier, P.H.J., Rancourt, D.G., Robert, J.-L., Berman, R.G., Redhammer, G.J., 2005. Fundamental difference between geometric homo-octahedral vs. geometric meso-octahedral sheets. Am. Mineral. 90, 399–410. https://doi.org/10.2138/am.2005.1609.

Miyata, S., 1983. Anion-exchange properties of hydrotalcite-like compounds. Clay Clay Miner. 31, 305–311. https://doi.org/10.1346/CCMN.1983.0310409.

Momma, K., Izumi, F., 2011. VESTA 3 for three-dimensional visualization of crystal, volumetric and morphology data. J. Appl. Crystallogr. 44, 1272–1276. https://doi.org/10.1107/S0021889811038970.

Monkhorst, H.J., Pack, J.D., 1976. Special points for Brillouin-zone integrations. Phys. Rev. B 13, 5188–5192. https://doi.org/10.1103/PhysRevB.13.5188.

Moraes, P.I.R., Wypych, F., Leitão, A.A., 2019. DFT study of layered double hydroxides with cation exchange capacity: (A+(H2O)6)[M62+Al3(OH)18(SO4)2]·6H2O (M2+ = Mg, Zn and A+ = Na, K). J. Phys. Chem. C 123, 9838–9845. https://doi.org/10.1021/acs.jpcc.9b00470.

Ortega-Castro, J., Hernández-Haro, N., Muñoz-Santiburcio, D., Hernández-Laguna, A., Sainz-Díaz, C.I., 2009. Crystal structure and hydroxyl group vibrational frequencies

of phyllosilicates by DFT methods. J. Mol. Struct. THEOCHEM 912, 82–87. https://doi.org/10.1016/j.theochem.2009.02.013. The 6th Congress on Electronic Structure: Principles and Applications (ESPA 2008).

Palin, E.J., Dove, M.T., Hernández-Laguna, A., Sainz-Díaz, C.I., 2004. A computational investigation of the Al/Fe/Mg order-disorder behavior in the dioctahedral sheet of phyllosilicates. Am. Mineral. 89, 164–175. https://doi.org/10.2138/am-2004-0119.

Perdew, J.P., Burke, K., Ernzerhof, M., 1996. Generalized gradient approximation made simple. Phys. Rev. Lett. 77, 3865–3868. https://doi.org/10.1103/PhysRevLett.77.3865.

Pérez-Sánchez, G., Galvão, T.L.P., Tedim, J., Gomes, J.R.B., 2018. A molecular dynamics framework to explore the structure and dynamics of layered double hydroxides. Appl. Clay Sci. 163, 164–177. https://doi.org/10.1016/j.clay.2018.06.037.

Pimentel, C., Pina, C.M., Sainz-Díaz, C.I., 2021. DFT simulations of the structure and cation order of norsethite, BaMg(CO3)2. ACS Earth Space Chem. 5, 1486–1497. https://doi.org/10.1021/acsearthspacechem.1c00058.

Pisson, J., Morel, J.P., Morel-Desrosiers, N., Taviot-Guého, C., Malfreyt, P., 2008. Molecular modeling of the structure and dynamics of the interlayer species of ZnAlCl layered double hydroxide. J. Phys. Chem. B 112, 7856–7864. https://doi.org/10.1021/jp800574d.

Plançon, A., 2001. Order-disorder in clay mineral structures. Clay Miner. 36, 1–14. https://doi.org/10.1180/000985501547286.

Richardson, M.C., Braterman, P.S., 2007. Infrared spectra of oriented and nonoriented layered double hydroxides in the range from 4000 to 250 cm-1, with evidence for regular short-range order in a synthetic magnesium−aluminum LDH with Mg:Al = 2:1 but not with Mg:Al = 3:1. J. Phys. Chem. C 111, 4209–4215. https://doi.org/10.1021/jp064744w.

Sainz-Díaz, C.I., Timon, V., Botella, V., Hernandez-Laguna, A., 2000. Isomorphous substitution effect on the vibration frequencies of hydroxyl groups in molecular cluster models of the clay octahedral sheet. Am. Mineral. 85, 1038–1045. https://doi.org/10.2138/am-2000-0719.

Sainz-Díaz, C.I., Cuadros, J., Hernández-Laguna, A., 2001. Analysis of cation distribution in the octahedral sheet of dioctahedral 2:1 phyllosilicates by using inverse Monte Carlo methods. Phys. Chem. Miner. 28, 445–454. https://doi.org/10.1007/s002690100171.

Sainz-Díaz, C.I., Timón, V., Botella, V., Artacho, E., Hernández-Laguna, A., 2002. Quantum mechanical calculations of dioctahedral 2:1 phyllosilicates: effect of octahedral cation distributions in pyrophyllite, illite, and smectite. Am. Mineral. 87, 958–965. https://doi.org/10.2138/am-2002-0719.

Sainz-Díaz, C.I., Palin, E.J., Hernández-Laguna, A., Dove, M.T., 2004a. Effect of the tetrahedral charge on the order-disorder of the cation distribution in the octahedral sheet of smectites and illites by computational methods. Clay Clay Miner. 52, 357–374. https://doi.org/10.1346/CCMN.2004.0520311.

Sainz-Díaz, C.I., Villacampa, A., Otálora, F., 2004b. Crystallographic properties of the calcium phosphate mineral, brushite, by means of First Principles calculations. Am. Mineral. 89, 307–313. https://doi.org/10.2138/am-2004-2-308.

Schaftenaar, G., Noordik, J.H., 2000. Molden: a pre- and post-processing program for molecular and electronic structures*. J. Comput. Aided Mol. Des. 14, 123–134. https://doi.org/10.1023/A:1008193805436.

Shannon, R.D., 1976. Revised effective ionic radii and systematic studies of interatomic distances in halides and chalcogenides. Acta Crystallogr. Sect. A 32, 751–767. https://doi.org/10.1107/S0567739476001551.

Sideris, P.J., Nielsen, U.G., Gan, Z., Grey, C.P., 2008. Mg/al ordering in layered double hydroxides revealed by multinuclear NMR spectroscopy. Science 321, 113–117. https://doi.org/10.1126/science.1157581.

Timón, V., Sainz-Díaz, C.I., Botella, V., Hernández-Laguna, A., 2003. Isomorphous cation substitution in dioctahedral phyllosilicates by means of ab initio quantum mechanical calculations on clusters. Am. Mineral. 88, 1788–1795. https://doi.org/10.2138/am-2003-11-1219.

Tkatchenko, A., Scheffler, M., 2009. Accurate molecular Van Der Waals interactions from ground-state electron density and free-atom reference data. Phys. Rev. Lett. 102, 073005 https://doi.org/10.1103/PhysRevLett.102.073005.

Vanderbilt, D., 1990. Soft self-consistent pseudopotentials in a generalized eigenvalue formalism. Phys. Rev. B 41, 7892–7895. https://doi.org/10.1103/PhysRevB.41.7892.

Vucelic, M., Jones, W., Moggridge, G.D., 1997. Cation ordering in synthetic layered double hydroxides. Clay Clay Miner. 45, 803–813. https://doi.org/10.1346/CCMN.1997.0450604.

Wang, J., Kalinichev, A.G., Kirkpatrick, R.J., Hou, X., 2001. Molecular modeling of the structure and energetics of hydrotalcite hydration. Chem. Mater. 13, 145–150. https://doi.org/10.1021/cm000441h.

Wang, J., Kalinichev, A.G., Amonette, J.E., Kirkpatrick, R.J., 2003. Interlayer structure and dynamics of Cl-bearing hydrotalcite: far infrared spectroscopy and molecular dynamics modeling. Am. Mineral. 88, 398–409. https://doi.org/10.2138/am-2003-2-316.

Warren, M.C., Dove, M.T., Myers, E.R., Bosenick, A., Palin, E.J., Sainz-Diaz, C.I., Guiton, B.S., Redfern, S.a.T., 2001. Monte Carlo methods for the study of cation ordering in minerals. Mineral. Mag. 65, 221–248. https://doi.org/10.1180/002646101550235.

Zhitova, E.S., Yakovenchuk, V.N., Krivovichev, S.V., Zolotarev, A.A., Pakhomovsky, Y.A., Ivanyuk, G.Y., 2010. Crystal chemistry of natural layered double hydroxides. 3. The crystal structure of Mg,Al-disordered quintinite-2H. Mineral. Mag. 74, 841–848. https://doi.org/10.1180/minmag.2010.074.5.841.